Atmospheric escape

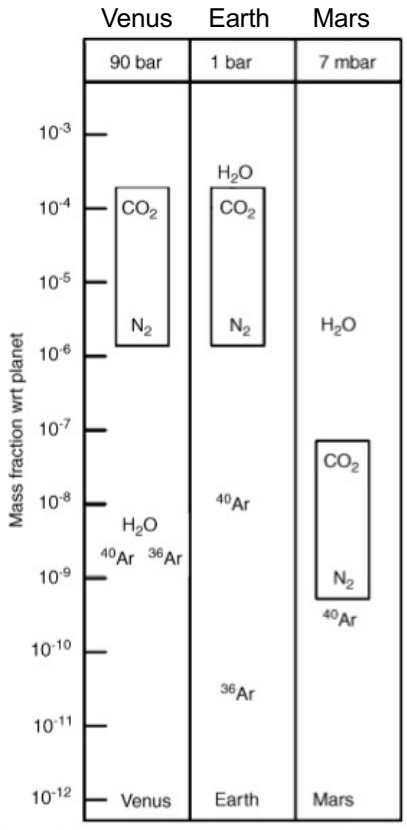

Fig. 1. Mass fraction with respect to planetary mass of volatiles on the terrestrial planets (by taking into account all known reservoirs, in particular terrestrial carbonates for CO_2).

Chassefiere et al. (2007)

Volatile species on the terrestrial planets

- The amount of H_2O on Venus is 1000-10000 times smaller than those of Mars and Earth.
- The amounts of CO_2 and N_2 on Mars are 1000 times smaller than those on Earth and Venus.

Escape processes

Thermal escape 熱的散逸

- Jeans' escape
  - Individual molecules in the high tail of the velocity distribution may reach escape velocity, at a level in the atmosphere where the mean free path is comparable to the scale height, and leave the atmosphere.
- Hydrodynamic escape
  - Heating by solar EUV（extreme-ultraviolet）radiation leads to expansion of the thermosphere to high altitudes.
  - Population of light species such as hydrogen in the upper atmosphere leads to expansion of the thermosphere to high altitudes.
  - Under such conditions, the pressure gradient pushes the atmosphere to interplanetary space. Because of the decrease of the gravitational acceleration at far distances, the atmosphere escapes as a fluid.

Nonthermal escape 非熱的散逸

- Dissociative recombination
- Charge exchange
- Pick-up
- Sputtering

Jeans escape

The condition for the escape to space of a molecule with mass *m* against the gravitational potential is

$$\int_{r_0}^{\infty} -m\frac{GM}{r^2}dr + \frac{mv^2}{2} > 0 \ ,$$

where *v* is the radial velocity and r^0 is the radial distance from the center of the planet. Then the escape velocity v_{esc} is obtained as

$$v > \sqrt{\frac{2GM}{r_0}} > v_{esc}$$

The high-energy tail of the Maxwellian distribution of the velocity distribution satisfies this condition, allowing the molecules to escape to space.

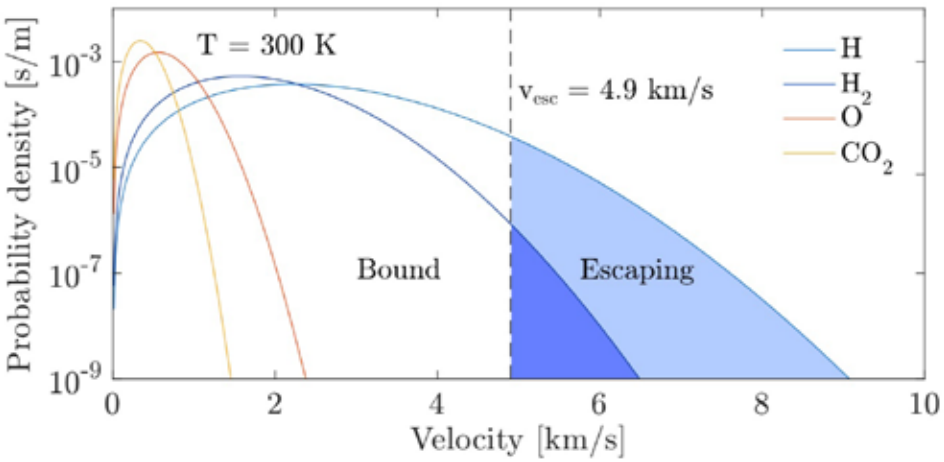

Figure 1.7: Thermal velocity distributions for several species in an example 300 K gas as described by the Maxwellian function (eq. 1.8). Only the H and H_2 distributions exhibit significant fractions above escape velocity near the exobase (4.9 km/s, marked by dashed line), in this case 0.023 % for H_2 and 2.1% for H. However, the Maxwellian distribution is isotropic, thus half these percentages will return to the atmosphere.

A simple solution of hydrodynamic escape (Parker model)

The atmosphere (including the solar corona) can be accelerated from subsonic near the surface to supersonic at far distances

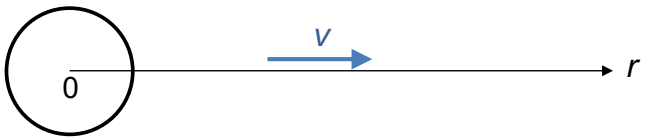

Letting the pressure be *p,* the mass density be *ρ*, the velocity be *v*, the gravity constant be *G*, and the planetary mass be *M*, the governing equations are:

$$\frac{1}{\rho}\frac{dp}{dr} + v\frac{dv}{dr} + \frac{GM}{r^2} = 0$$

$$4\pi r^2 \rho v = const.$$

$$p = \rho RT$$

Assuming that the temperature T does not depend on the distance r, we have

$$\frac{1}{v}\left(\frac{v^2}{c_s^2}-1\right)\frac{dv}{dr}=\frac{2}{r}-\frac{GM}{c_s^2}\frac{1}{r^2} \qquad c_s = RT \quad \text{~sound speed}$$

At the point where $v = c_s$, dv/dr goes to infinity unless the RHS becomes zero there. Therefore, we assume the RHS becomes zero at $r = r_c$ where $v = c_s$. Then we have

$$r_c = \frac{GM}{2c_s^2}$$

In this case, $dv/dr > 0$ is satisfied both at $r < r_c$ and $r > r_c$, enabling the velocity to be accelerated from subsonic to supersonic.

In the solar wind, letting $T = 10^6$ K, the velocity exceeds the sound speed at $r_c = 8\text{x}10^6$ km (5% of the Sun-Earth distance).

Solutions of hydrodynamic escape

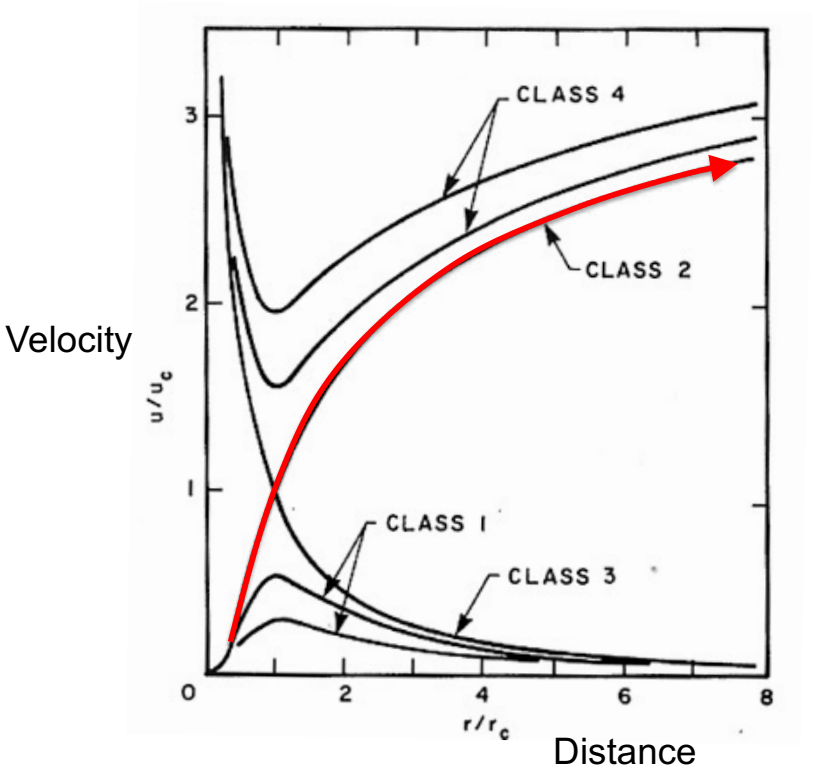

Velocity

Distance

Energy balance of the thermosphere

(Bougher et al. 1994)

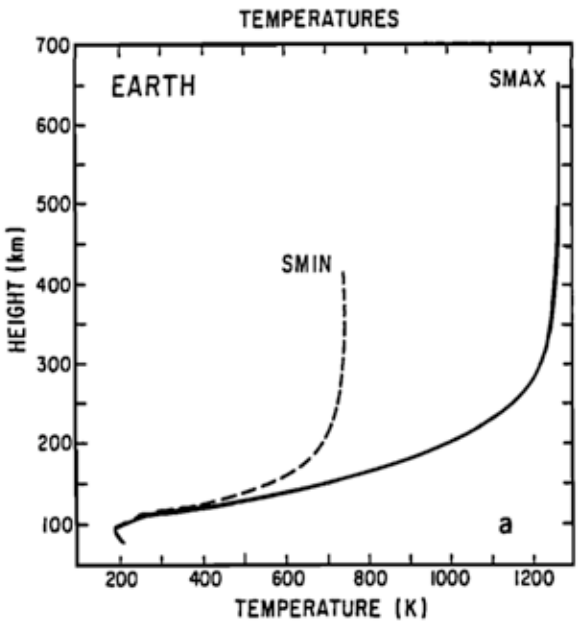

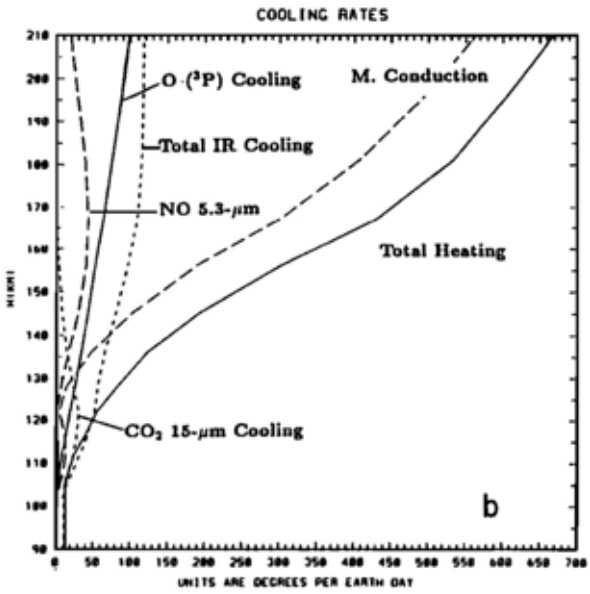

Source of solar UV

Solar spectrum

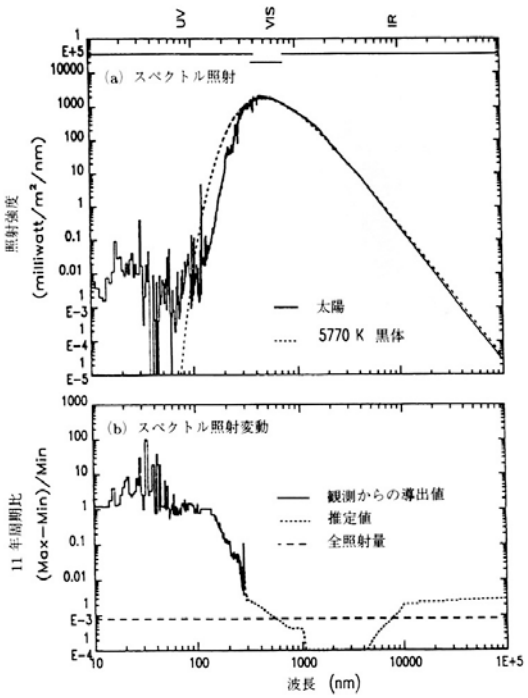

（ブレッケ，超高層大気物理学）

Structure of the solar atmosphere

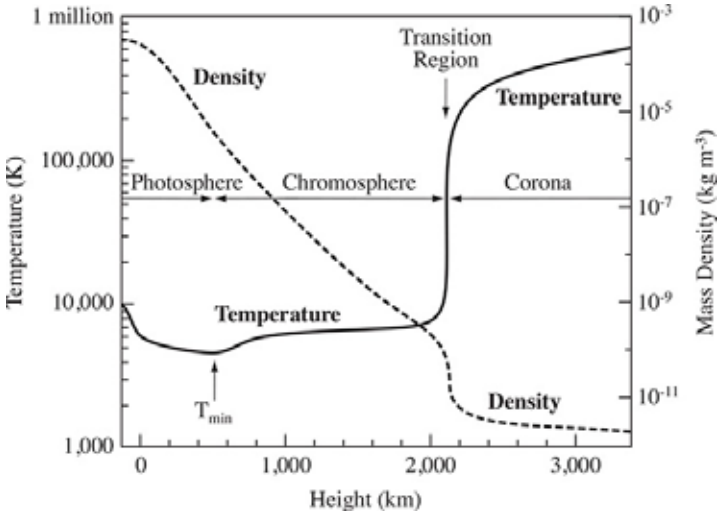

(Eugene Avrett, Smithsonian Astrophysical Observatory)

Solar dynamo

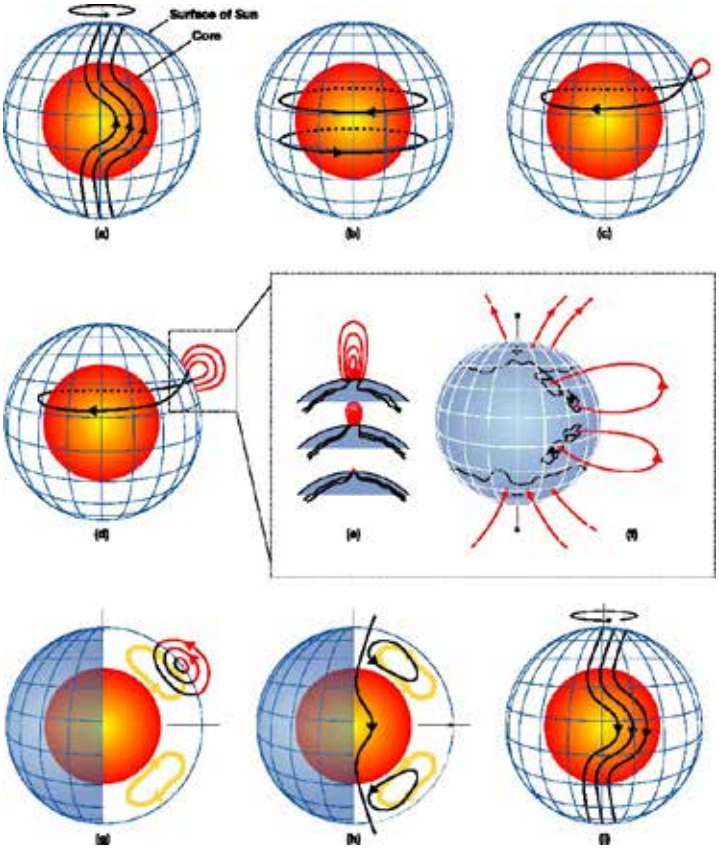

Dikpati & Gilman (2009)

Table 1. Physical parameters and age-rotation relation of well observed and studied solar proxies in comparison with the Sun (after Güdel, 2007). L_X refers to a range of 0.1–2.4 keV as measured by the ROSAT satellite.

Star name	Type	Mass [M_{Sun}]	Radius [R_{Sun}]	$\log\left(\frac{L_X}{L_{bol}}\right)$	Rot. [days]	Age [Ga]
HD 129333 [EK Dra]	G1.5 V	1.06	0.95	−3.61	2.68	0.1
HD 72905 [π^1 UMa]	G1.5 V	1.03	0.95	−4.47	4.9	0.3
HD 206860 [HN Peg]	G0 V	1.06	0.99	−4.52	4.86	0.3
HD 39587 [χ^1 Ori]	G1 V	1.01	0.96	−4.65	5.24	0.3
HD 1835 [BE Cet]	G2 V	0.99	1.02	−4.46	7.65	0.6
HD 20630 [κ^1 Cet]	G5 V	1.02	0.93	−4.73	9.21	0.65
HD 114710 [β Com]	G0 V	1.08	0.925	−5.52	12	1.6
HD 190406 [15 Sge]	G5 V	1.01	1.1	−5.64	13.5	1.9
Sun	G2 V	1	1	−6.29	25.4	4.6
HD 146233 [18 Sco]	G2 V	1.01	1.03	—	23	4.9
HD 128620 [α Cen A]	G2 V	1.1	1.22	−6.67	~30	5–6
HD 2151 [β Hyi]	G2 IV	1.1	1.9	−6.41	~28	6.7
HD 186408 [16 Cyg A]	G1.5 V	1	1.16	—	~35	8.5

Table 5. Solar radiation flux enhancement as function of wavelength normalized to the present solar flux value from present to 3.9 Gyr ago (Ribas *et al.*, 2005; Güdel, 2007).

Solar age [Gyr]	t b.p. [Gyr]	X-ray [1–20 Å]	SXR [20–100 Å]	EUV [100–920 Å]	FUV [920–1180 Å]	Lyman-α [1200–1300 Å]	UV [1300–1700 Å]
4.6	0	1	1	1	1	1	1
3.2	1.4	2	1.6	1.5	1.4	1.3	—
2.6	2	3	2	1.9	1.6	1.5	—
1.9	2.7	6	3	2.7	2.1	1.9	2.4
1.1	3.5	16	6	5.1	3.4	2.8	—
0.7	3.9	37	11	8.6	5	3.9	—

Lammer et al. (2012)

Stellar evolution

- UV radiation from the Sun-like stars originates in magnetic chromospheric and transition-zone regions which are heated to temperatures of $\sim 10^4$– 10^5 K. Magnetic activity driven by the star's rotation is believed to be critical for this heating.
- For stars with masses ≤1.5M_{Sun} and ages of about a few 100 Myr, angular momentum loss by a stellar wind brakes rotation. The rotation period of the young Sun was much faster (~few days) during the first 500 Myr after the arrival at the main sequence.
- The radiation and plasma history of our Sun can be separated into a period of a moderate decrease from about 4 Gyr ago to the present and a very early extreme period of about 500 Myr after the young Sun arrived at the main sequence.

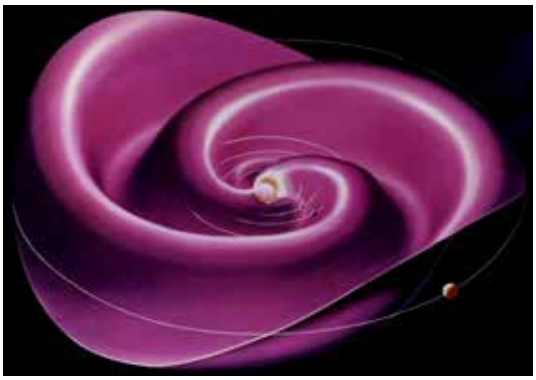

© ESA

Evolution of stellar activity

- The fluxes of X-ray, EUV, solar wind, and CME (coronal mass ejection) decrease with the deceleration of the star's rotation.
- Stars with small masses maintain high activity for a long time.

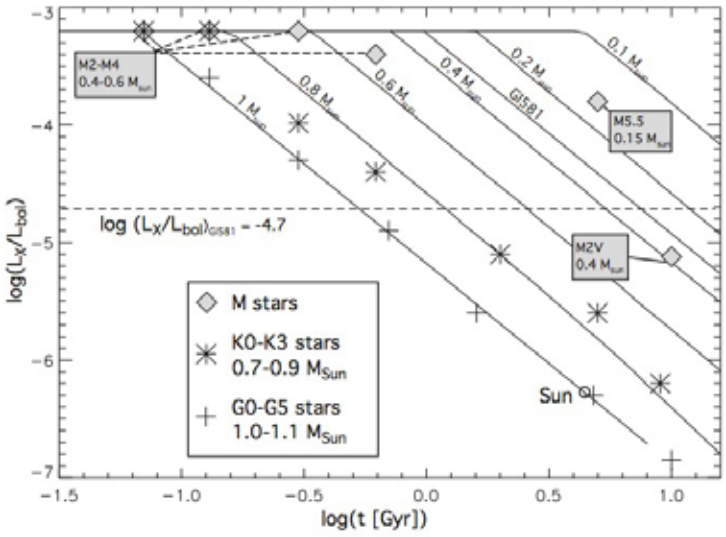

Selsis et al. (2007)

Fig. 5. Evolution of the ratio between the X-ray and bolometric luminosities as a function of age for stars of different masses. The solid lines represent semi-empirical laws, while symbols give observed values for G (+), K (∗) and M (◇) stars. The dashed line gives the upper limit for the value of $\log(L_X/L_{bol})$ in the case of Gl 581, for which there is no ROSAT detection.

Response of the Earth's and Venus' thermosphere to changes of solar EUV flux

Lammer et al. 2008

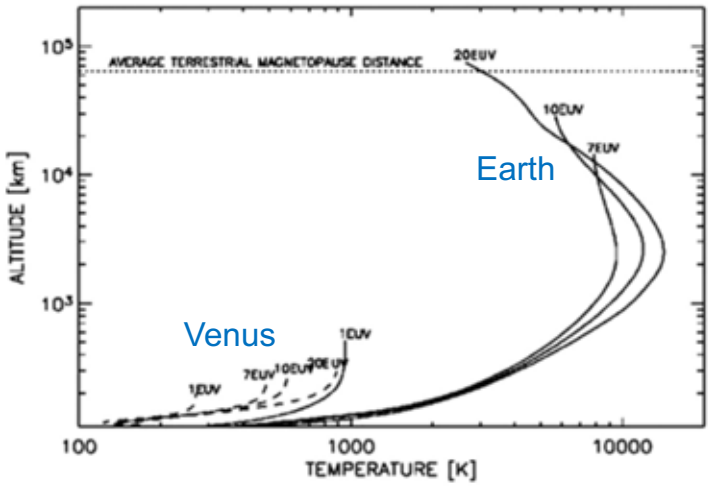

Fig. 6 Thermospheric temperature profiles between 100 km and the corresponding exobase levels for present (=1), 7, 10 and 20 times higher EUV solar fluxes than today, applied to Venus (Kulikov et al. 2006) and Earth (Tian et al. 2008) with the present time atmospheric composition. The efficient IR-cooling due to large amount (96%) of CO_2 in the hydrostatic thermosphere of Venus yields much lower exobase temperatures and atmospheric expansion compared with an Earth-like atmospheric composition

Tian et al. (2008)

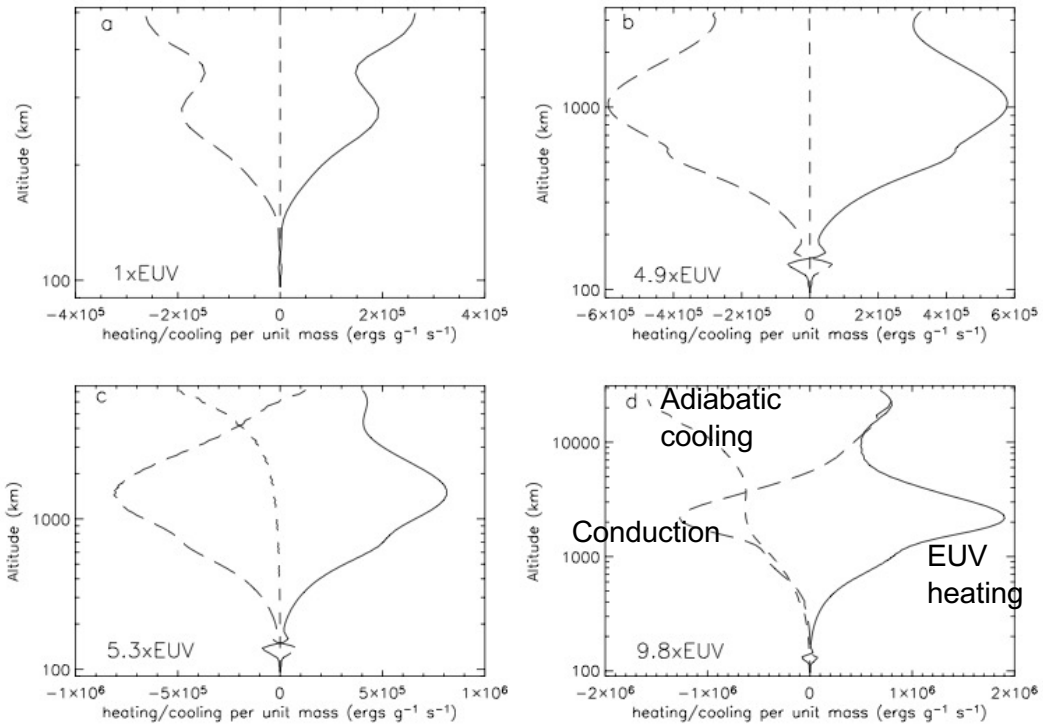

Figure 7. Profiles of heating and cooling mechanisms under different solar EUV flux cases (normalized by the solar EUV energy flux at solar mean). The solid curves are the net heating from radiative transfer calculations, including both the heating terms and IR cooling terms described in section 3. The long dashed curves are the molecular thermal conduction, and the short dashed curves are the adiabatic cooling.

Escape of hydrogen from Early Venus

- Increase of the water mixing ratio in the lower atmosphere leads to high population of hydrogen in the thermosphere, thereby driving hydrodynamic escape.

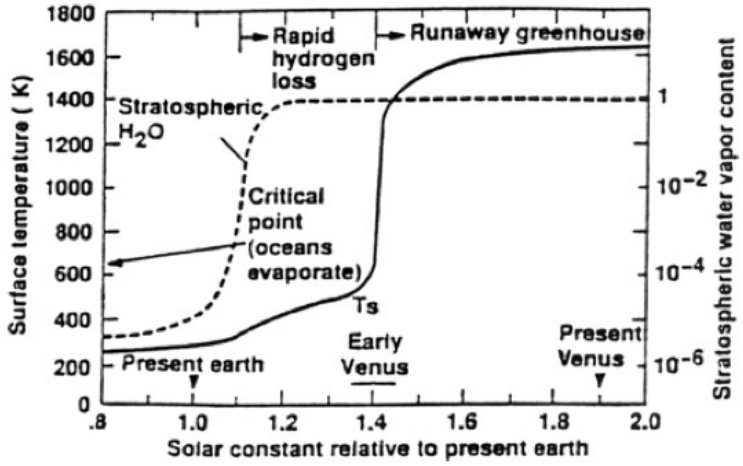

Fig. 1 Diagram illustrating what would happen to Earth if it were slowly pushed inwards towards the Sun. The *horizontal scale* is the solar flux relative to its value at 1 AU. The *solid curve* represents mean global surface temperature (*left-hand scale*). The *dashed curve* represents stratospheric H_2O mixing ratio (*right-hand scale*). The solar flux at Venus today and at 4.5 billion years ago is indicated (adapted from Kasting 1988)

Lammer et al. (2008)

Long-term trend of solar luminosity

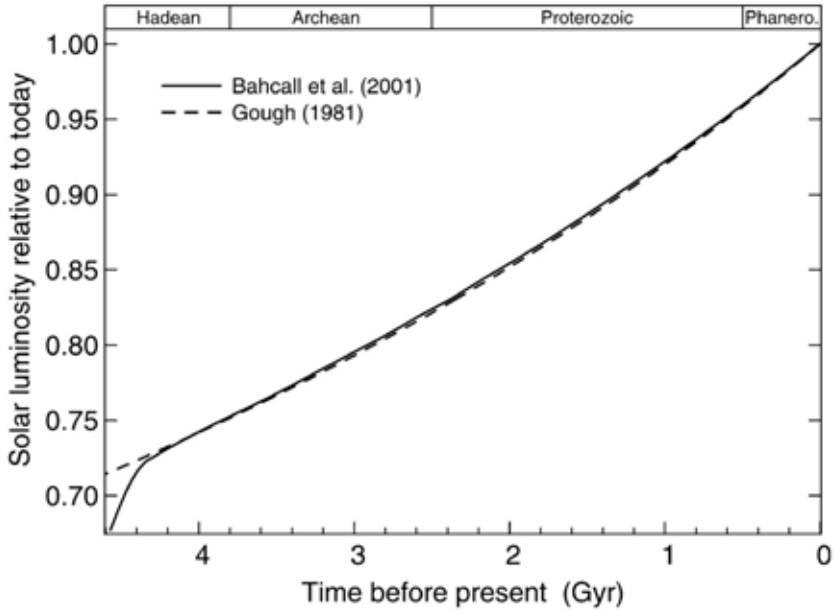

Feulner (2012)

Theoretical models for the stellar interior show that the luminosity of the Sun had to change over time, with the young Sun being considerably less luminous than today.

Change of the vertical structure of Earth's atmosphere with the change of the sea surface temperature

Nakajima et al. (1992)

Atmospheric temperature

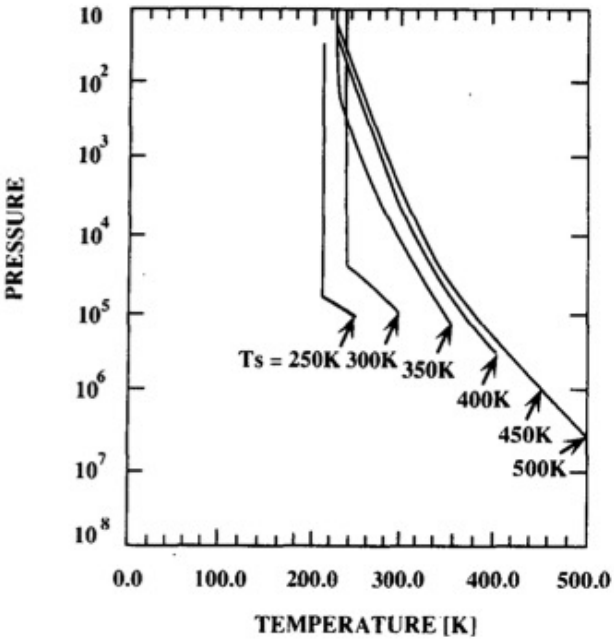

Water vapor mixing ratio

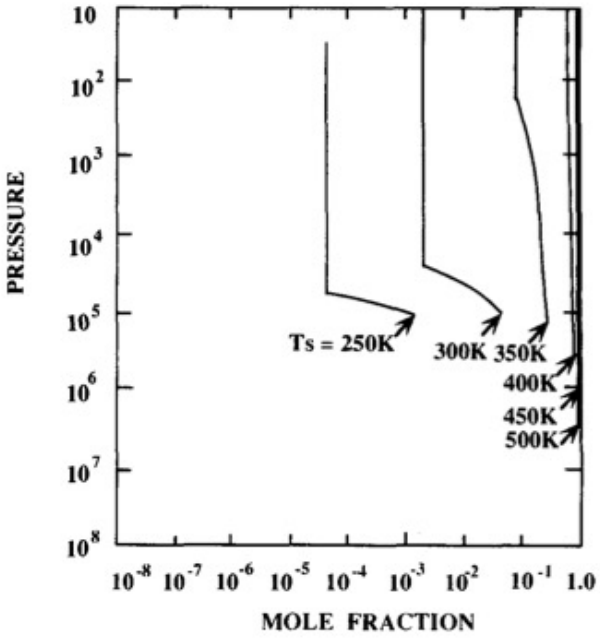

Kasting & Pollack (1983)

ESCAPE RATES FOR HIGH H_2O LEVELS

Case	$c_0(H_2O)$	$\Phi_{esc}(H)$ (cm^{-2} sec^{-1})	F (g $ster^{-1}$ sec^{-1})
A	7.2×10^{-4}	2.2×10^{9}	1.3×10^{3}
B	6.3×10^{-3}	3.8×10^{10}	2.3×10^{4}
C	5.5×10^{-2}	1.3×10^{11}	7.7×10^{4}
D	4.6×10^{-1}	2.7×10^{11}	1.6×10^{5}
	H_2O mixing ratio at the cold trap (90km,170K)	Calculated H flux	Calculated mass flux

→ Amount of Earth's ocean can escape in 2 billion years

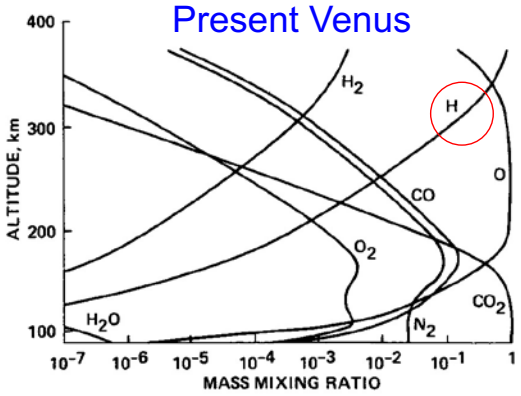

FIG. 2. Mass mixing profiles for the present Venus atmosphere.

Composition of the upper atmosphere

- The amount of H atoms in the thermosphere increases with the increase of water vapor in the lower atmosphere.
- Absorption of solar EUV by H atoms is the primary heat source.

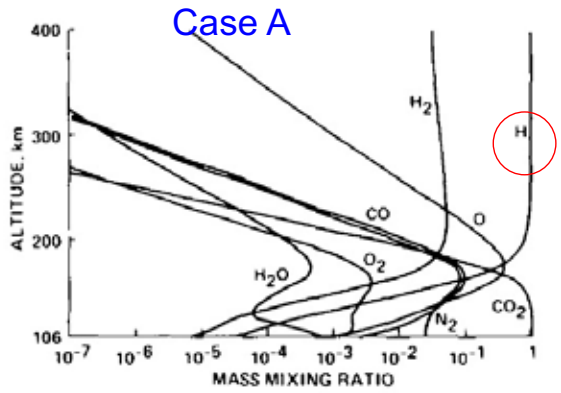

FIG. 9. Mass mixing ratio profiles for Case A.

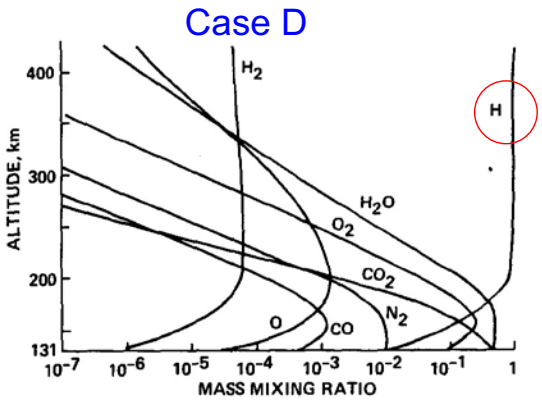

FIG. 10. Mass mixing ratio profiles for Case D.

- Terrestrial planets may evolve through phases where their upper atmospheres are hydrogen-rich.
- High H_2O mixing ratio levels and/or high XUV fluxes result in Φ_H (escape flux) in the range of about 10^{11}–10^{13} cm^{-2} s^{-1}.

Kulikov et al. (2006)

Table 4
Escape fluxes of atomic hydrogen during hydrodynamic conditions from Venus' upper atmosphere as a function of various mesopause H_2O mixing ratios c_{H_2O} and solar XUV flux (see Kasting and Pollack, 1983)

c_{H_2O}	0.00072	0.0063	0.055	0.46
XUV flux ϕ_H ($cm^{-2}\,s^{-1}$)				
1	$\sim 2.2 \times 10^{9}$	$\sim 3.8 \times 10^{10}$	$\sim 1.3 \times 10^{11}$	$\sim 2.7 \times 10^{11}$
2	$\sim 6.5 \times 10^{9}$	$\sim 9.3 \times 10^{10}$	$\sim 3.2 \times 10^{11}$	$\sim 6.6 \times 10^{11}$
4	$\sim 1.0 \times 10^{10}$	$\sim 1.8 \times 10^{11}$	$\sim 6.2 \times 10^{11}$	$\sim 1.3 \times 10^{12}$
8	$\sim 1.8 \times 10^{10}$	$\sim 3.2 \times 10^{11}$	$\sim 1.0 \times 10^{12}$	$\sim 2.3 \times 10^{12}$
16	$\sim 2.8 \times 10^{10}$	$\sim 4.9 \times 10^{11}$	$\sim 1.7 \times 10^{12}$	$\sim 3.5 \times 10^{12}$
100	$\sim 2.2 \times 10^{11}$	$\sim 3.8 \times 10^{12}$	$\sim 1.3 \times 10^{13}$	$\sim 2.7 \times 10^{13}$

Chemical composition of the early terrestrial atmosphere

Hashimoto et al. (2007)

Formation of a reducing atmosphere from CI-like material ?

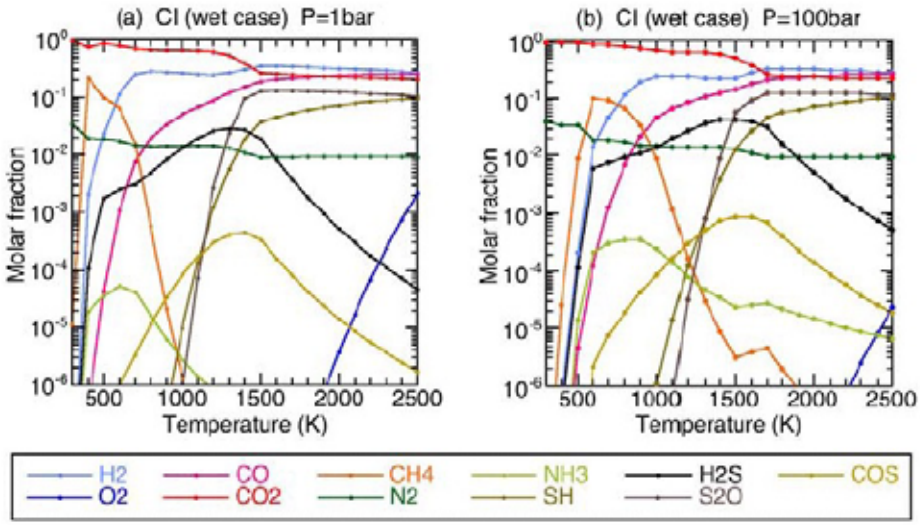

Figure 1. Equilibrium composition of dry gas phase at (a) 1 bar and (b) 100 bar total pressures. Water content in CI chondrite is about 20 wt% (wet case). This figure does not include water vapor since atmospheric water varies greatly due to condensation.

Loss of Oxygen ?

Lammer et al. (2008)

- In the case of an intense hydrodynamic escape of atomic hydrogen, the theory predicts that heavy atoms can be dragged off along with escaping H atoms.
- In the case of a purely EUV-driven hydrodynamic escape, the removal of all (or most of) the oxygen contained in an Earth-sized ocean was possible only at very early times (t < 30–40 Myr).
- Another possible loss mechanism caused by solar wind interaction with an upper atmosphere is non-thermal escape.

Titan's hydrodynamically-escaping atmosphere

- hydrodynamic escape driven principally by solar UV heating by CH_4 absorption

Lammer et al. (2012)

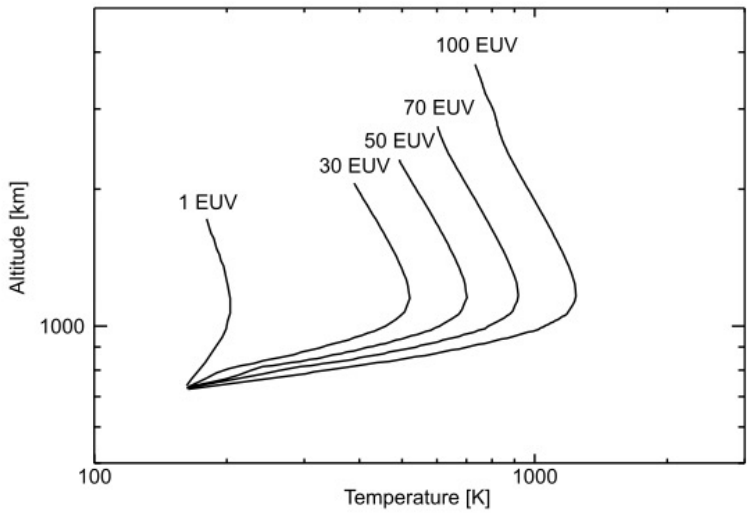

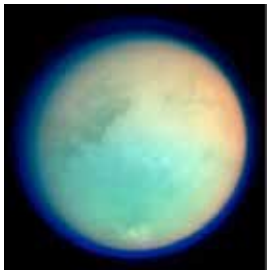

Fig. 8. Thermospheric temperature profiles between the mesopause and the corresponding exobase levels for 1 (present), 30, 50, 70, 100 times higher EUV solar fluxes than today, expected at Saturn's large satellite Titan with the present time atmospheric composition.

Non-thermal escape (1)

- Charge exchange
  - Slow neutral + fast ion → **fast neutral** + slow ion

    (such as $H + H^{+*} \rightarrow H^{+} + H^{*}$)
  - By exchanging charge, the fast ion (which was trapped by the planet's magnetic field) becomes a neutral and is able to escape.
- Photochemical reactions
  - Conversion of the energy of absorbed EUV/X-ray to kinetic energy

    (such as $O_2^{+} + e \rightarrow O^{*} + O^{*}$)
- Sputtering
  - Impact of fast ions (solar wind or trapped particles) knocks atoms out of the atmosphere

Non-thermal escape (2)

- Ion escape
  - Ions flow upward along polar field lines via **ambipolar diffusion** and escape down magnetic field lines
  - Occurs in magnetospheres and also at Mars
- Ion pickup
  - If the exobase is above the boundary between the solar wind flow and the planet, once the particles become photoionized they can be picked up directly by the solar wind flow and carried away

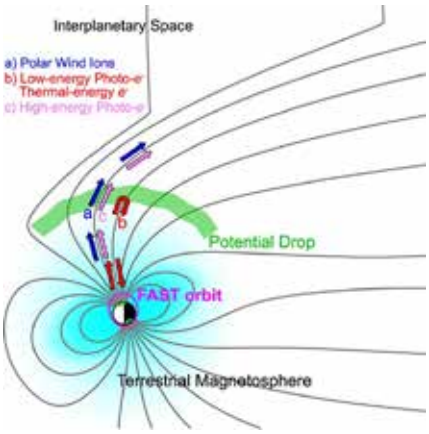

Kitamura et al. (2015)

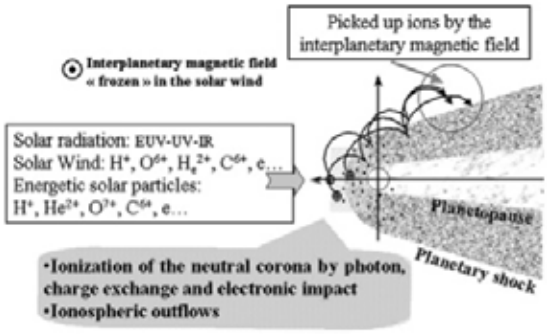

Lammer et al. (2008)

Ion pick-up

Wei et al. (2017)

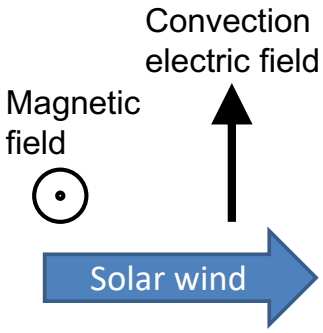

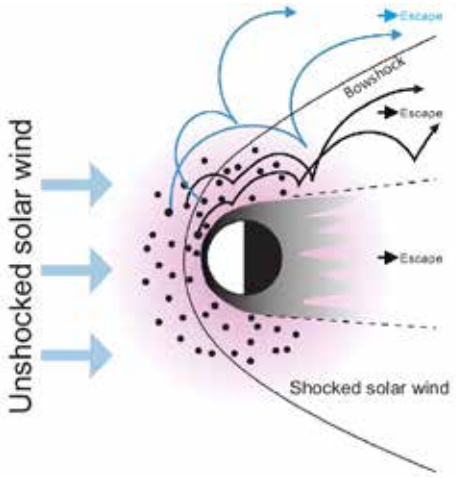

Lorentz force acting on atmospheric ions

$$\mathbf{F} = q(\mathbf{E} + \mathbf{v} \times \mathbf{B})$$

Convection electric field

$$\mathbf{E}_{mot} = -\mathbf{v}_{sw} \times \mathbf{B}_{IMF}$$

Pickup ions move initially in the direction of the solar wind convection electric field

v_{sw} : solar wind velocity
B_{IMF} : interplanetary magnetic field

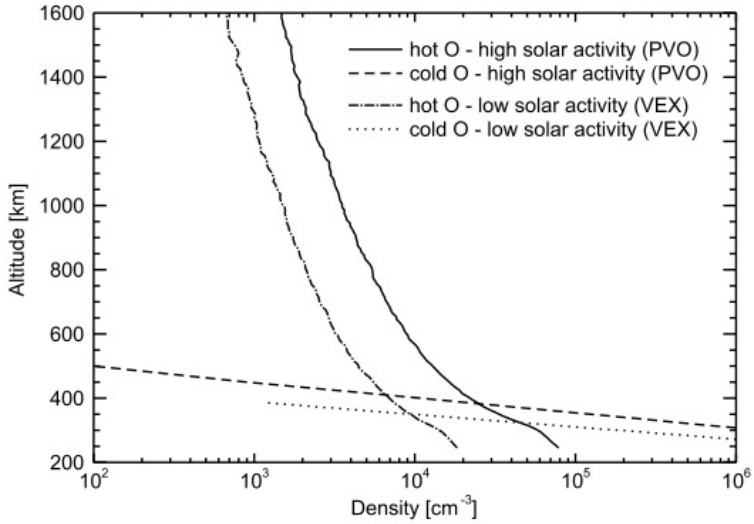

Fig. 9. Photochemically produced supra-thermal "hot" O atom density profiles at present Venus during low and high solar activity conditions compared with the bulk atmosphere.

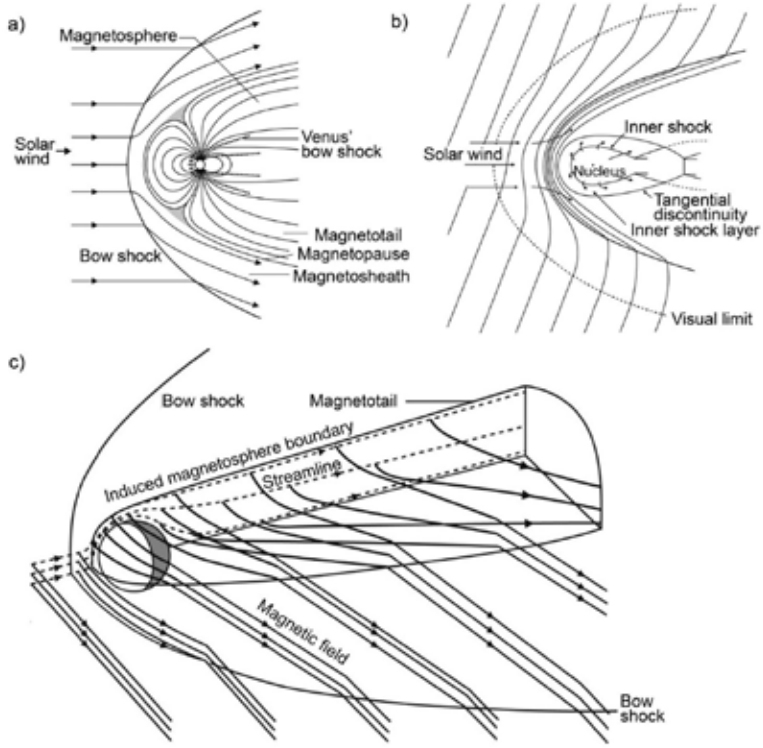

Different magnetospheres

Fig. 5 Comparison of three different magnetospheres. The Earth's magnetosphere (**a**) is a typical example of an intrinsic magnetosphere. Venus magnetosphere is overlaid as a *dashed line* to illustrate the difference in size (adopted from Luhmann 1991a). A cometary induced magnetosphere is characterized by the draping of the solar wind magnetic field (**b**) introduced by the mass loading process (adopted from Russell et al. 2016). The induced magnetosphere of Venus (**c**) is a typical example of a magnetosphere of unmagnetized atmospheric object (adopted from Saunders and Russell 1986). Solar wind interaction to Mars exhibits similar interaction to Venus

Futaana et al. (2017)

Non-thermal escape from Mars

- Escape of oxygen from the present Mars was observed by Phobos spacecraft.
- The observed escape rate was such that the total oxygen in the current CO_2 atmosphere is lost in 100 million years (or the total oxygen in a 1m-depth ocean is lost in 4.5 billion years.)

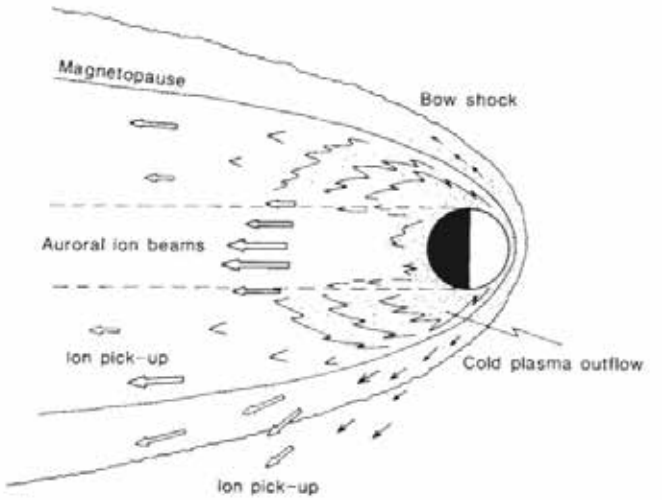

Lundin et al. (1989)

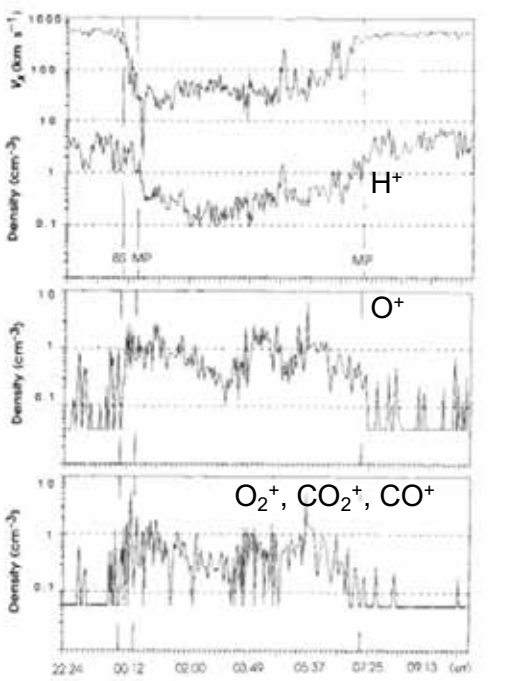

FIG. 2. Moment parameters for O^+ and H^+ ions during the second Phobos 2 orbit around Mars (4–5 February 1989). The top panel gives the flow velocity and the number density of H^+ ions. The middle and lower depict the number density of O^+ and molecular ions (O_2^+, CO_2^+, CO^+), respectively. The inbound bow shock (BS) and magnetopause (MP), and the outbound magnetopause crossings are marked by vertical lines.

Bulk plasma escape

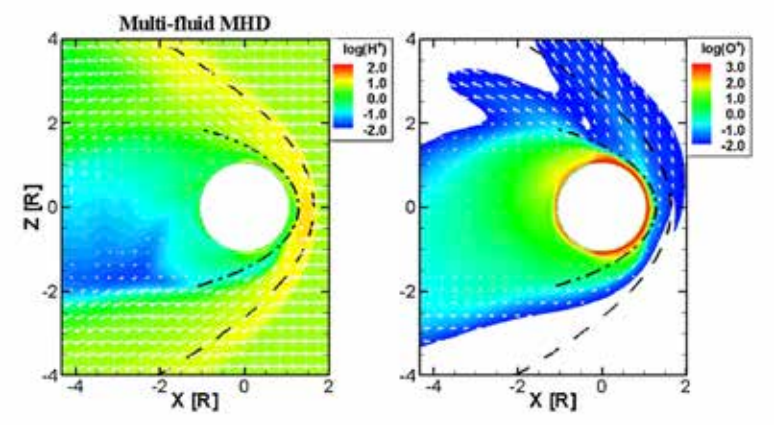

Ma et al. 2004, Najib et al. 2011

K-H (shear) instability

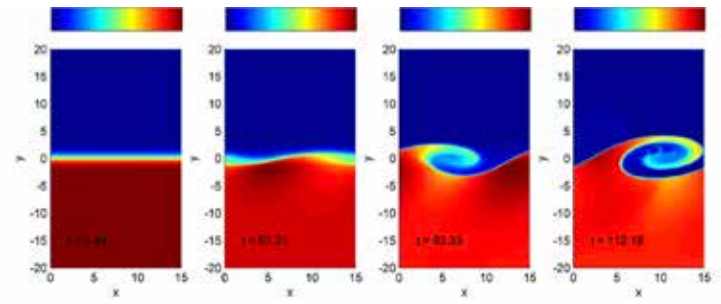

Fig. 12 Nonlinear evolution of the Kelvin-Helmholtz instability. The time series of the mass density is shown, from an MHD simulation with periodic boundary conditions in the x-direction. The mass density changes from the upper to the lower plasma layer and exhibits an increase of up to ten times (see the color code; *blue*: low density, *red*: high density). In the upper layer, the plasma flows from *left* to *right*. In the lower layer, the plasma is at rest. Initially small perturbations of the boundary layer separating the two plasma layers

Escape from the present Mars observed by Mars Express/ASPERA (Carlsson et al., 2006)

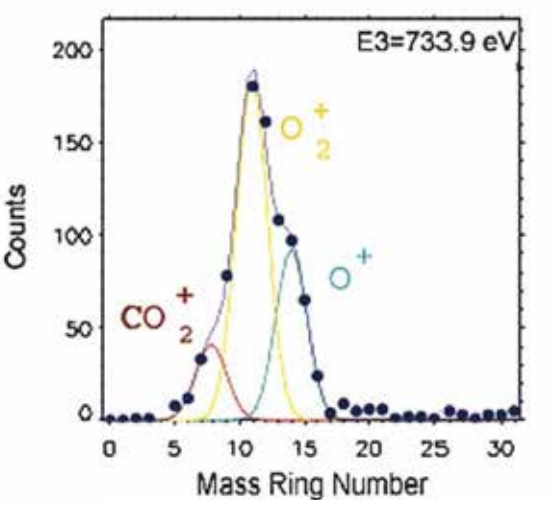

←重い　　軽い→
原子・分子の質量数

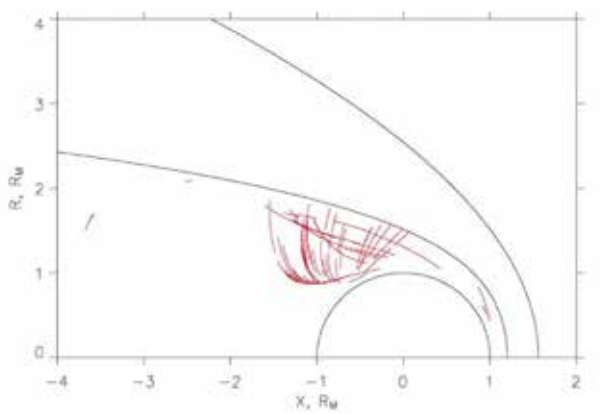

Fig. 6. Pieces of the orbits corresponding to the time intervals of all ion-beam events used in this study.

Ratio of escape rates
$O^+:O_2^+:CO_2^+ \sim 9 : 9 : 2$

Escape of molecular ions, which have been believed to be unable to escape due to large masses, was observed.

Sputtering at Mars

Leblanc & Johnson 2002

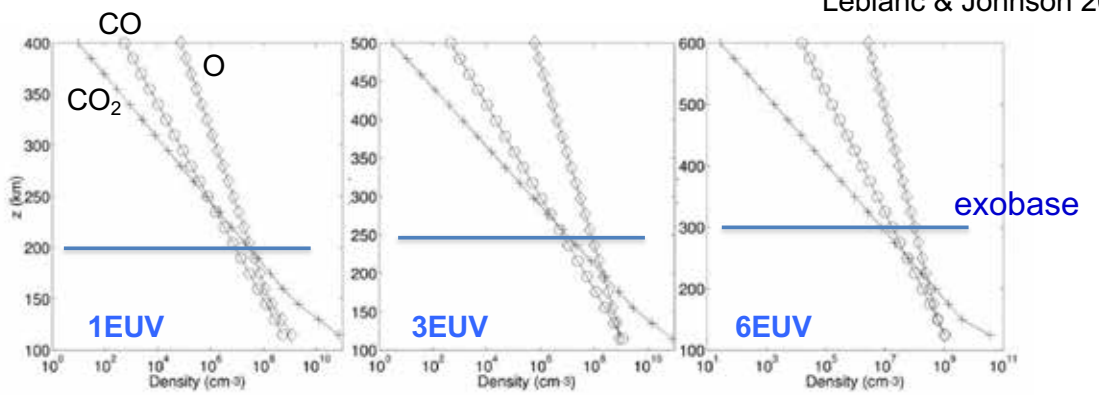

Figure 1. Density profiles of the main species composing the Martian atmosphere between 400, 500, and 600 km and 115 km in altitude for the (left) 1 EUV case, (middle) 3 EUV case, and (right) 6 EUV case, respectively. Diamonds, O atom; circles, CO molecule; and crosses, CO_2 molecule.

Table 1. Efficiency of Incident O^+ Pickup Ions in Ejecting Atmospheric Particles

	Epochs of Martian History		
	1 EUV	3 EUV	6 EUV
Multispecies Molecular Atmosphere			
Yield of O	0.86	1.66	1.99
Yield of CO_2	0.12	0.05	0.02
Yield of CO	0.09	0.06	0.06
Yield of C	0.22	0.24	0.33
Total atomic yields	1.6	2.2	2.5

Atmospheric escape from present Venus

Lammer et al. (2008)

Table 3 Thermal and non-thermal loss rates of oxygen and hydrogen from present Venus

Escape process	Loss [s^{-1}] 1 EUV
Jeans: H	2.5×10^{16} (1)
Photochemical reactions: H	3.8×10^{25} (1)
Electric field force: H^+	$\leq 7 \times 10^{25}$ (2)
Solar wind ion pick up: H^+	1×10^{25} (1)
Solar wind ion pick up: H_2^+	$< 10^{25}$ (1)
Solar wind ion pick up: O^+	1.5×10^{25} (1)
Detached plasma clouds: O^+	5×10^{24}–10^{25} (1, 3)
Sputtering: O	6×10^{24} (4)
Cool plasma outflow: O^+	$\leq 10^{26}$ (5)

(1) Lammer et al. (2006a); (2) Hartle and Grebowsky (1993); (3) Terada et al. (2002); (4) Luhmann and Kozyra (1991); (5) Barabash et al. (2007)

Evolution of escape rates

Chassefiere et al. (2007)

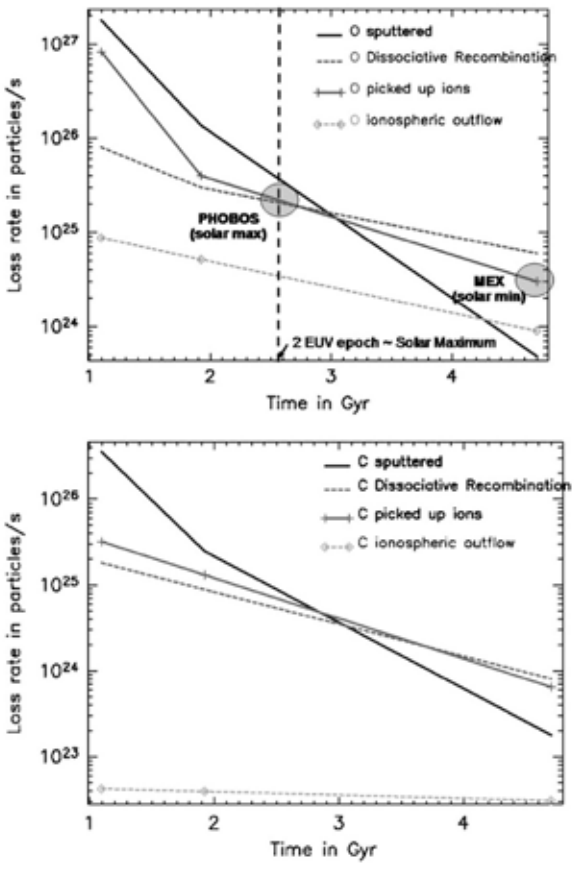

Fig. 4. Evolution of the escape rate of oxygen (upper panel) and of carbon (lower panel) due to non-thermal mechanisms of escape applied to the Martian atmosphere (estimated as described in the text). On the upper panel are also indicated the measured escape rate of total ion oxygen (probably the sum of the ion escape and ionospheric outflow) reported by Lundin et al. (1989) for solar maximum conditions (from ASPERA on Phobos spacecraft) and the escape rate recently estimated from ASPERA electron measurements on board Mars Express for solar minimum conditions (Sauvaud A., personal communication).

Volatile escape from Mars

The amounts of CO_2 and N_2 on Mars are 1000 times smaller than those on Earth and Venus, while ^{40}Ar, which is considered to have degassed after the planet's formation, exists with a similar amount. This implies that Martian CO_2 and N_2 have been lost just after the planet's formation.

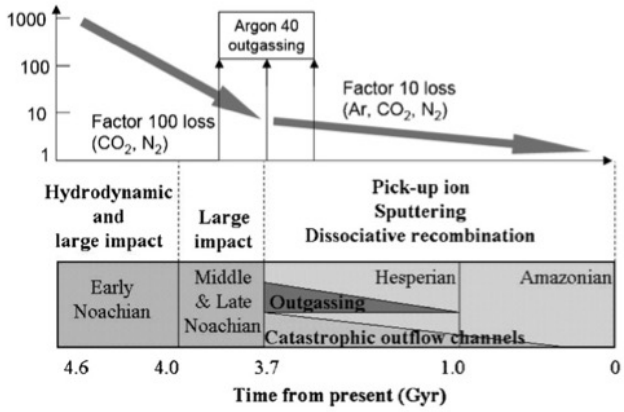

Chassefiere et al. (2007)

Fig. 3. Schematic chronology of atmospheric escape on Mars. A factor of 100 loss is expected to have occurred during the heavy bombardment period, by impact loss and possibly hydrodynamic escape. In the subsequent period, by using radiogenic argon as a tracer of sputtering escape, an additional loss by a typical factor of 10 occurred.

O^+ outflows from Earth, Mars and Venus

Ramstad & Barabash (2021)

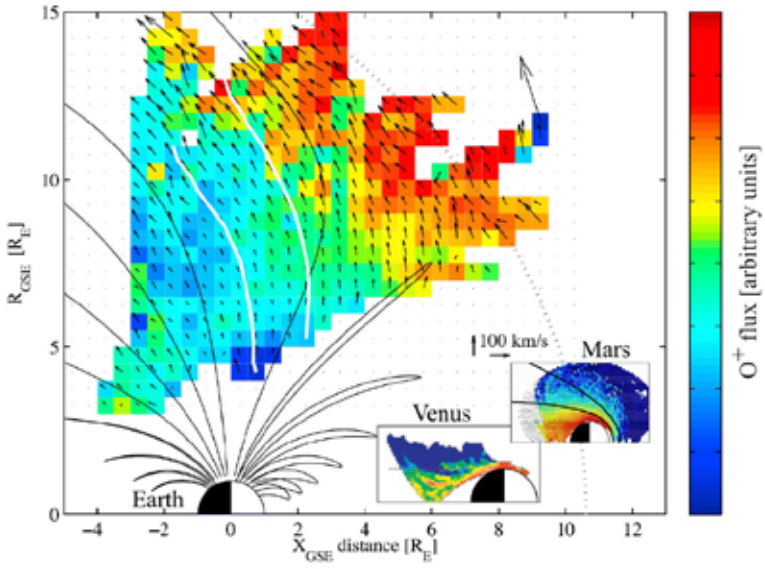

Fig. 4 Time-averaged O^+ outflows from Earth mapped in cylindrical coordinates, with analogous maps for Venus and Mars mapped inlaid on the same scale, contrasting the scale of the outflow and interaction area with the solar wind (Earth's magnetopause shown as dotted line) imposed by Earth's intrinsic magnetic dipole field, compared to the smaller induced magnetospheres of Venus and Mars. Red colors show high fluxes and blue colors show low fluxes in all maps, though the absolute values differ. Adapted from Nilsson et al. (2012a), Fedorov et al. (2008), and Ramstad (2017)

Ramstad & Barabash (2021)

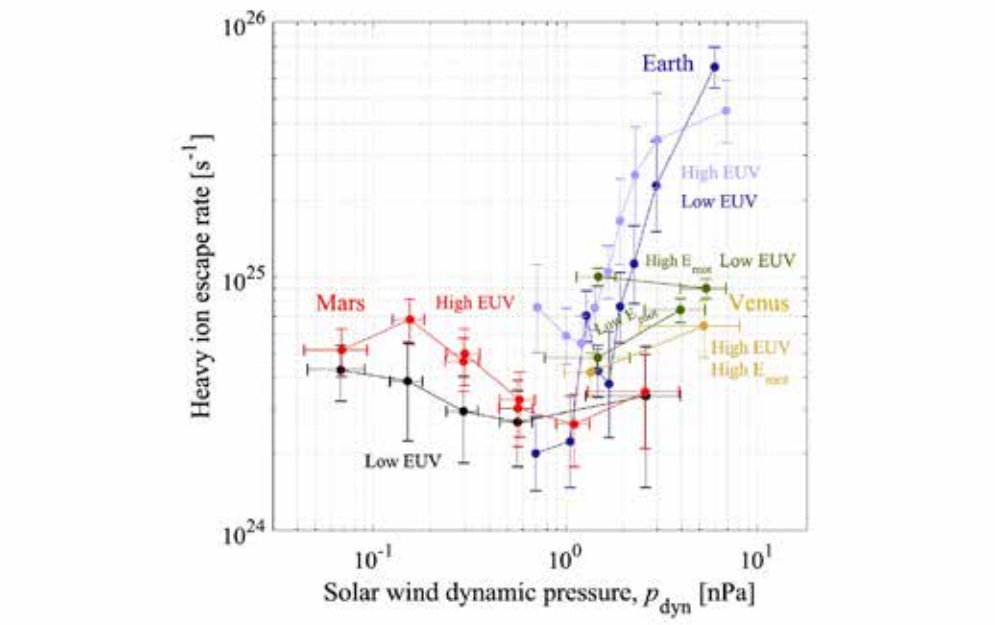

Fig. 8 Escape rates of heavy ions ($M/q \geq 16$) from Venus (Masunaga et al. 2019), Earth (Schillings 2019), and Mars (Ramstad et al. 2018); as dependent on upstream solar wind dynamic pressure for individually constrained ranges of solar EUV. At Venus, Masunaga et al. (2019) divide the VEX dataset in time as before/after 31 Dec. 2010, corresponding to the transition from solar minimum to maximum and an abrupt increase in the F10.7 index, a solar EUV proxy. At Earth, Schillings (2019) divides the Cluster dataset by below/above a solar 0–90 nm EUV intensity of 3.5 mW/m^2. At Mars, Ramstad et al. (2018) map escape rates over a 2D upstream parameter space, here we show the estimated escape rates from Mars for solar 0–118 nm photon flux above 4.7×10^{14} m^{-2} s^{-1} (red) and below 3.5×10^{14} m^{-2} s^{-1} (black), separately

Energy- and Supply-Limited Escape

- Limiting factors:
  - Energization rate ∝ solar wind power
  - Ion supply rate ∝ photochemical production rate of ions

- Comparison among the planets shows (Ramstad & Barabash 2021):
  - Ion escape from Venus and Earth is energy-limited, while the ion escape from Mars is supply-limited. (For Mars, the required escape energy is small enough that all the energy required to maintain escape is already provided. ?)
  - Mars gravity is low enough that oxygen can escape via EUV-driven dissociative recombination reaction $O^{+2} + e^- \rightarrow 2O^* + E$, which can produce oxygen atoms with kinetic energies sufficient to escape the shallow Martian gravity well. (yet not sufficient to facilitate oxygen escape from Earth or Venus)

Role of intrinsic magnetosphere

- (Ramstad & Barabash 2021) Contrary to the classical idea that the magnetic dipole protects the Earth's atmosphere, the comparison with Venus and Mars suggests that an intrinsic magnetic dipole field is not required to prevent stellar wind-driven escape of planetary atmospheres. The presence of dipole field may instead increase the rate of ion escape.
- The dipole increases the solar wind interaction area, thereby facilitating the a higher rate of energy transfer from the solar wind to atmospheric ions. ?

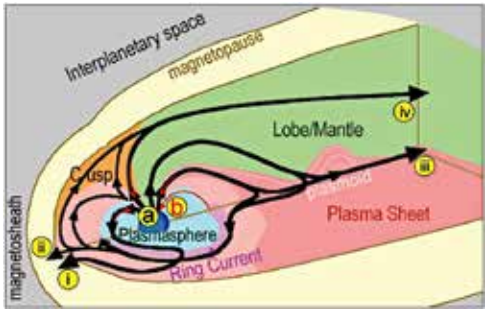

Illustration of atmospheric ion escape in the Earth's intrinsic magnetosphere adapted from Seki et al. (2001)

Mars Atmosphere and Volatile EvolutioN (MAVEN) mission

Arrive at Mars : September 21, 2014

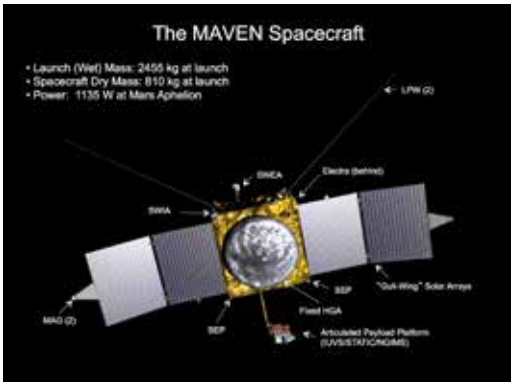

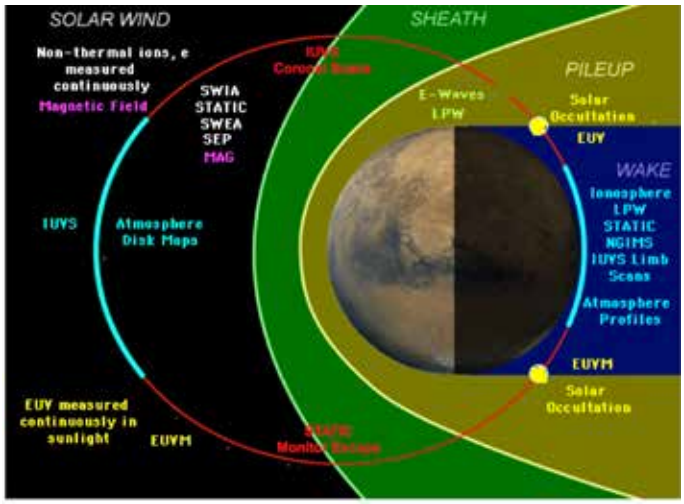

MAVEN Science instruments

- NGIMS (Neutral Gas and Ion Mass Spectrometer)
  - He, N, O, CO, N2, O, O2, Ar and CO2, and their major isotopes
  - thermal O+2 , CO+2 , NO+, O+, CO+, C+, N+2 , OH+, and N+
- LPW (Langmuir Probe and Waves)
  - thermal electron density and temperatures
  - electric field wave power at frequencies important for ion heating
- STATIC (Supra-thermal and Thermal Ion Composition)
  - major ions (H+, O+, O+2 , CO+2), their corresponding ion temperatures (~0.02 eV to >10 eV), and the 3-component (X,Y,Z) ion flow velocities (~0.2 to 25 km/s)
- IUVS (Imaging Ultraviolet Spectrometer)
  - H, C, N, O, CO, N2, and CO2
  - C+ and CO+2
- SEUV (Solar Extreme Ultraviolet)
  - solar irradiance at soft X-ray (0.1–7.0 nm), EUV (17–22 nm), and UV (Lyman-α) wavelengths
- SEP (Solar Energetic Particle)
  - energy spectrum and angular distribution of solar energetic electrons (30–300 keV) plus protons and heavier ions (30 keV–6 MeV)

Observations by MAVEN

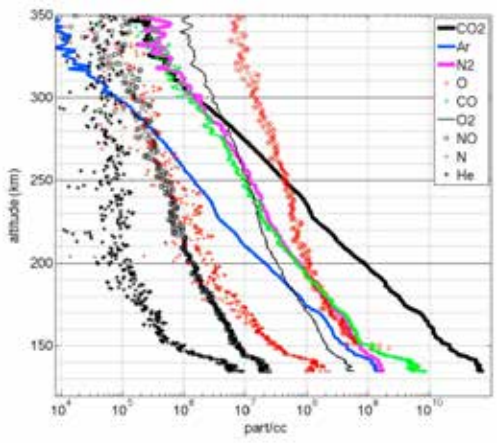

Figure 2.6: Density profiles of neutral species in the Martian upper atmosphere as measured by the NGIMS instrument on MAVEN near local noon (11:50 AM LST). Adapted from *Mahaffy et al.* [2015b] (CC-BY-NC-ND).

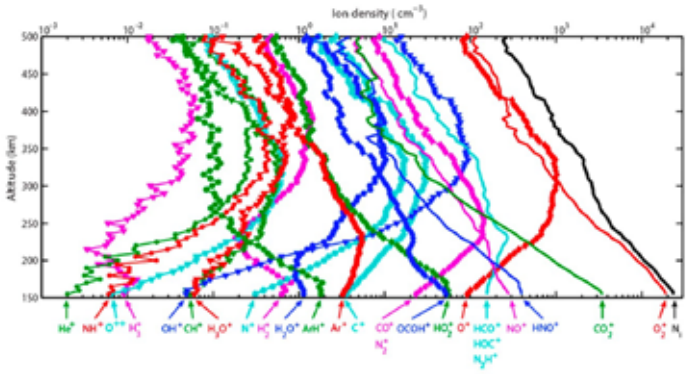

Figure 2.7: Density profiles of ionospheric species at Mars as measured by the NGIMS instrument on MAVEN at ca. 60° solar-zenith angle. Adapted from *Benna et al.* [2015], with permission.

Mahaffy et al. (2015)

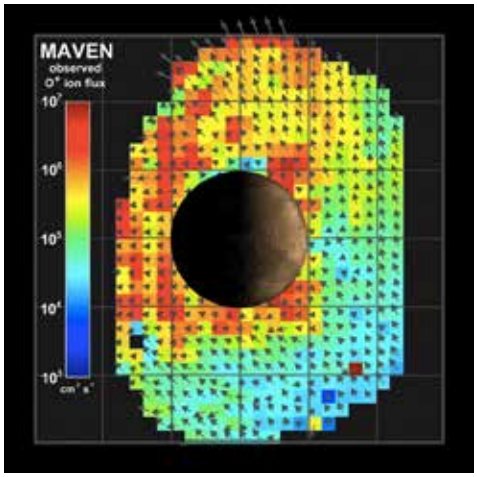

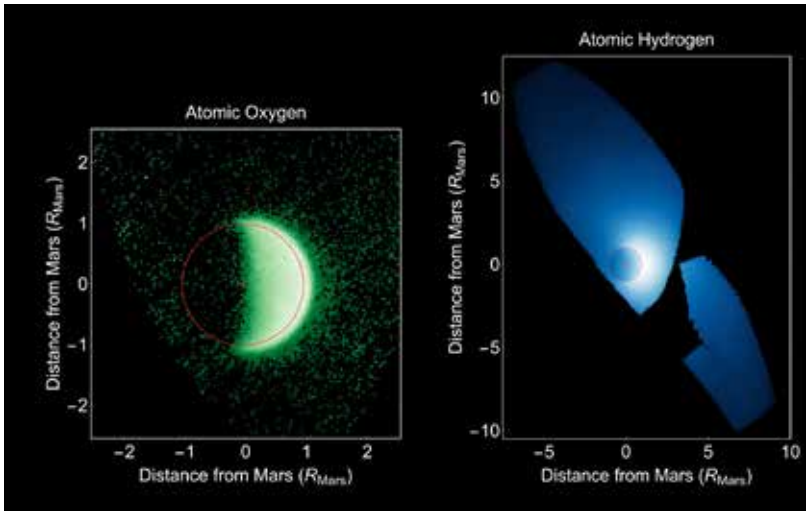

Discovery of diffuse aurora on Mars

Schneider et al. (2015)

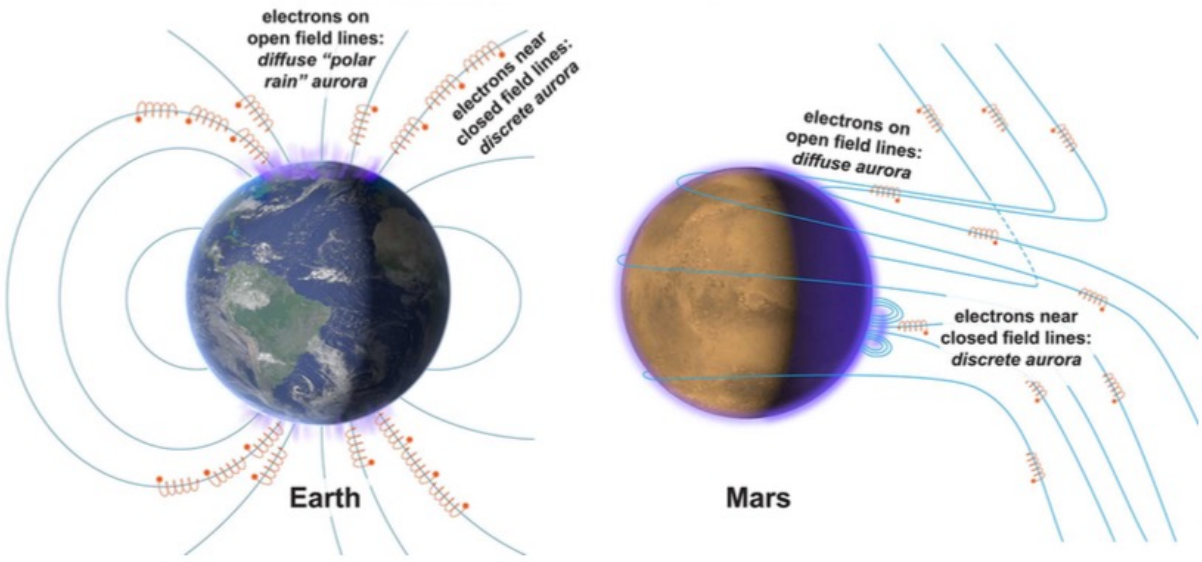

Fig. 5. Comparison of field geometry for diffuse and discrete auroras on Earth and Mars. Mars lacks an internally generated global magnetic field, due to the cooling of its core. Fields surrounding Mars are a combination of small structures locked in the crust billions of years ago (lower right) and solar wind field lines draped around the planet.

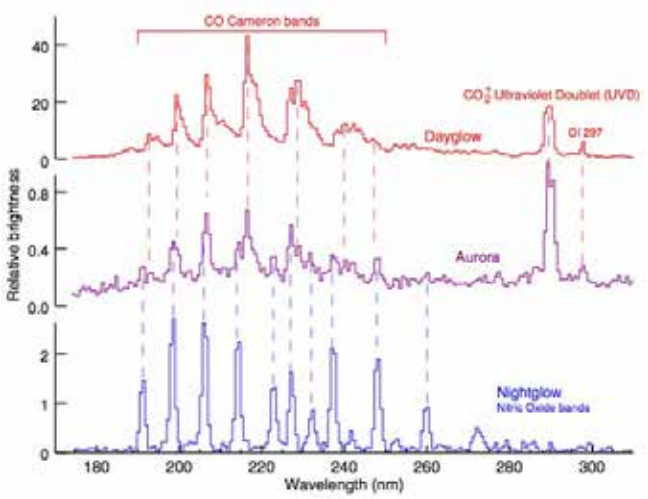

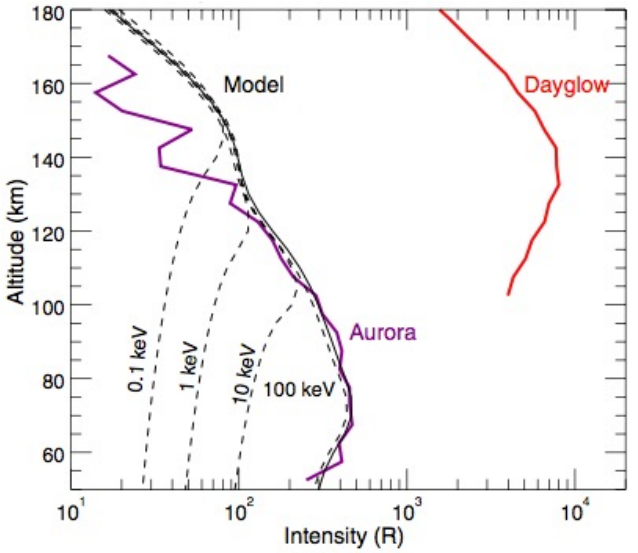

“Diffuse auroras may have additional effects on atmospheric processes. Only a fraction of the deposited energy results in atmospheric excitation and emission. Incident particles also ionize and dissociate atmospheric species, as well as heat the target atmosphere. These effects can lead to increased atmospheric escape rates: Ionized particles at sufficient altitudes can escape via outflow processes, and atmospheric heating can lead to increased thermal escape. “